Supporting information

Pore-interface Engineering Improves Doxorubicin loading to Triazine-based Covalent Organic Framework

Preeti Rathi[†], Sumanta Chowdhury[‡], Partha Pratim Das[#], Anubha Chaudhary[†] and Prem F. Siril[‡]*

[†]School of Biosciences and Bioengineering and Bio-X Research Centre, Indian Institute of Technology Mandi, Mandi, 175005, Himachal Pradesh, India

[‡]School of Chemical Sciences and Advanced Materials Research Centre, Indian Institute of Technology Mandi, Mandi, 175005, Himachal Pradesh, India

[#]Department of Chemistry, Manipal Institute of Technology, Manipal Academy of Higher Education, Manipal, 576104, Karnataka, India.

Supporting information

Figure S10. FTIR spectra of (a) DOX-loaded NTzCOF (b) DOX-loaded CTzCOF and (c) DOX-loaded TzCOF along with DOX and pristine COF.

Figure S11. O1s XPS spectra of three pristine COFs, DOX-loaded COFs and DOX.

Figure S12. N1s XPS spectra of three pristine COFs, DOX-loaded COFs and DOX.

Figure S13. Confocal images of A549 cells treated with NTzCOF at different z-height.

Figure S14. Confocal images of A549 cells treated with DOX at different time intervals.

S1. Materials and characterization

Materials

Doxorubicin hydrochloride ($C_{27}H_{29}NO_{11}$·HCl, , TCI Chemicals, AR, 95%), 2,4,6-tris(4-aminophenyl)-1,3,5-triazine (C24H21N3, TCI Chemicals, AR, 98% , TCI Chemicals), Hexamethylenetetramine ($C_6H_{12}N_4$, , Alfa Aesar, AR 99% , Alfa Aesar), Phloroglucinol ($C_6H_6O_3$, Avra, AR 98%), Trifluoroacetic acid (SRL, AR, 98.5%), Hydrochloric acid (SDFCL, 35-38%), Dichloromethane (Rankem, LR), Sodium Sulphate (SDFCL, AR, 99.7%), Ethanol (CSS, AR, 99.9%), 6-Amino-3-pyridinecarbonitrile ($C_5H_3NNH_2CN$, Aldrich, 97%), Trifluoromethanesulfonic Acid (CF_3SO_3H, 98%), Methanol (Rankem, LR), Sodium hydroxide (Loba chemie, 97%), Tetrahydrofuran (SDFCL, LR), n-Hexane (Rankem, HPLC), 1,4-dioxane (Fisher scientific, 99%), mesitylene (TCI chemicals, 97%), and Acetic acid (Loba chemie, 30%). All the purchased reagents and chemicals were used without any further purification.

Cell culture

Human embryonic kidney (HEK 293T) and lung adenocarcinoma (A549) cell lines (NCCS, Pune), Dulbecco's modified essential medium (DMEM, Gibco), FBS (fetal bovine serum, Gibco), L-glutamine (Gibco), Anti-Anti (Gibco), 3-(4,5-dimethylthiazol-2-yl)-2,5-diphenyl tetrazolium bromide (MTT, Sigma-Aldrich), Dimethyl sulfoxide (DMSO, Sigma-Aldrich), Fluoroshield^{TM} with DAPI (Sigma-Aldrich), Paraformaldehyde (Sigma-Aldrich).

Characterisation

The Fourier Transform Infrared (FTIR) spectra of the synthesized materials were acquired using a PerkinL160000C spectrum two FTIR spectrometer. The spectra consisted of 16 scans, covering a wavenumber range from 600 to 4000 cm^{-1} at a resolution of 1 cm^{-1}. Approximately 0.2 mg of the samples were carefully weighed and combined with a suitable quantity of KBr in a mortar. The mixture was thoroughly ground to achieve homogeneity using a pestle. Subsequently, the resulting powder was pressed into pellets using a Hydraulic Pellet Press and subjected to analysis using the FTIR spectrometer.

Powder X-ray diffraction (PXRD) was performed with a Cu-sealed tube (Cu K X-rays of 0.1541 nm wavelength) at 45 kV and 200 mA on a Rigaku Smart Lab 9kW rotating anode X-ray diffractometer. Diffraction patterns were recorded in the scanning range of 4.5-40° at a scan rate of 2°/min.

We employed the EXPGUI interface within the GSAS software suite to perform comprehensive profile fitting (Rietveld refinement) for the structural models of the COF

samples. This analysis covered samples synthesized under various conditions. For refining the experimental PXRD patterns of COF samples with a triclinic (P1) structure, we utilized crystal information files (CIF) obtained from simulations.

The Autosorb-iQ-MP/XR model from Quantachrome was employed to evaluate nitrogen physisorption isotherms at 77 K. Around 12-15 mg of dry COF samples were placed in 6 mm glass tubes and subjected to activation for 4 hours at 80 °C, following a ramp of 5 °C/min, and then at 120 °C with a ramp of 2 °C/min. Activation continued until the pressure change dropped below 30 millitorr. The apparent Brunauer-Emmett-Teller (BET) surface areas were calculated using AsiQwin software. Pore size distributions were determined using the "N_2 at 77 K on carbon, cylindrical pore, quenched solid density functional theory (QSDFT) equilibrium" model. The microporous surface area and volume were determined using the de Boer (v-t) method.

The morphology and statistical distribution of particle sizes in the freshly synthesized samples were assessed using Field Emission Scanning Electron Microscopy (FESEM, FEI Nova Nano SEM-450, 10 kV) and Transmission Electron Microscopy (TEM, FEI Tecnai, Tungsten filament, 200 kV). The procedure involved suspending the sample in ethanol and subjecting it to sonication for 10-20 minutes at room temperature. Subsequently, the suspension was drop-casted onto a clean carbon-supported copper TEM grid and left to air dry at room temperature.

X-ray photoelectron spectroscopic (XPS) experiments were carried out on a Thermo Fischer Scientific NEXSA XPS model using Al-Kα (1486.6 eV) X-ray radiation. The data was calibrated and analysed with Avantage software by using binding energy of C1s (~284.8 eV) as the internal reference. About ~1.5 mg sample was suspended in 500 µL ethanol and sonicated for 10 min at room temperature followed by drop casting it on top of a clean silicon wafer. The drop casted samples were then dried at room temperature.

Zeta potential measurements were done using Malvern Zeta Sizer-Nano ZS90 instrument at 25 °C for water and PBS and 37°C for DMEM.

The ^{1}H and ^{13}C NMR spectra were collected using a Jeol-ECX-spectrometer.

Fluorescence emission spectra of COFs were collected using Fluorolog-Horiba scientific at excitation wavelength of 472 nm for NTzCOF and 425 nm for TzCOF.

Absorbance spectra to calculate drug-loading were recorded using UV-1800 spectrophotometer (Shimadzu, Japan).

Microplate reader (InfiniteM200Pro) was used for MTT assay.

A1 Nikon confocal laser scanning microscope was used for fluorescence imaging.

S2. Synthesis procedure

S2.1 Synthesis of triformyl phloroglucinol (Tp) molecule

Synthesis of Tp was done in the laboratory according to the previously reported method with a minute modification.[1] Trifluoroacetic acid (TFA, 45 mL) was added to a mixture comprising hexamethylenetetramine (HMTA, 7.4 g, 52.5 mmol, 2.2 equiv.) and dried phloroglucinol (3 g, 23.8 mmol, 1 equiv.). The solution was heated under a nitrogen atmosphere at 100 ºC for 2.5 h. Following this, a gradual addition of HCl (3 M, 150 mL) was performed, and then heated with continuous stirring

at 100 ºC for 1 h. After cooling to room temperature, the reaction mixture underwent filtration through double filter paper. The resulting filtrate was subjected to dichloromethane extraction (4 × 100 mL), subsequent drying over anhydrous Na_2SO_4, and concentrated using rota-evaporator, yielding a dull orange-colored solid. This solid was washed repeatedly with hot ethanol to obtain a free-flowing powder with an off-white hue. Further, the product was purified using sublimation technique. The yield was calculated to be 18%. ^{1}H NMR (500 MHz, DMSO-d6): δ ppm 9.97 (s, 3H, CHO) [**Fig.S1**].

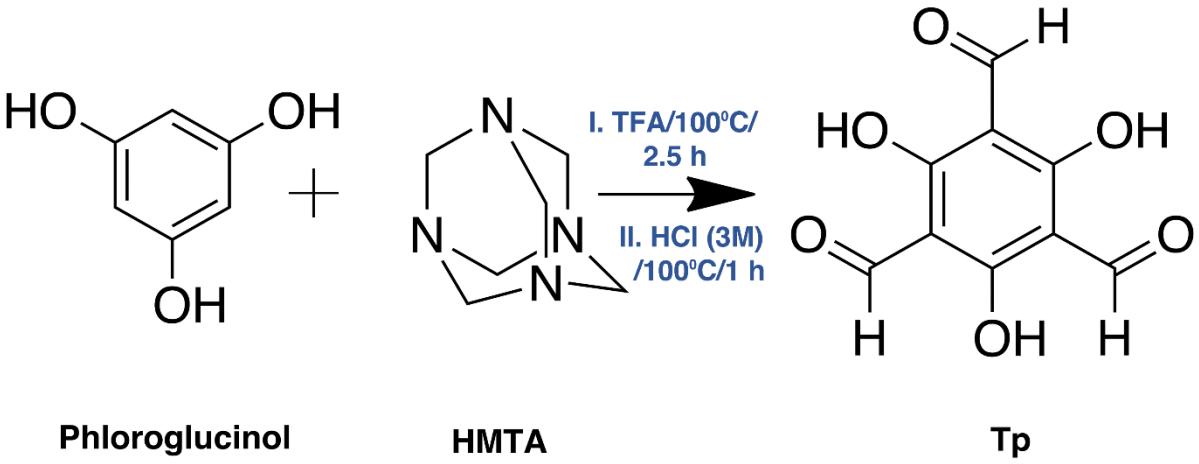

Scheme 1: Schematic diagram for synthesis of triformylphloroglucinol (Tp) by using phloroglucinol and HMTA.

S2.2 Synthesis of 5,5',5''-(1,3,5-triazine-2,4,6-triyl) tris(pyridin-2-amine):

TAPT-N was synthesized by following previously reported method.[2] A conventional synthesis method involved the use of a round-bottom flask to hold 4 mL (44.4 mmol) of trifluoromethanesulfonic acid (CF_3SO_3H), kept at -20 ºC. 6-Amino-3-pyridinecarbonitrile (0.772 g, 6.538 mmol) was added gradually in the CF_3SO_3H-filled round-bottom flask at -20 ºC. Once the addition concluded, the flask was allowed to warm to 0 ºC. Stirring of the resulting mixture occurred for a span of 2 days at 0 ºC in a nitrogen atmosphere. Subsequently, the reaction mixture was quenched by introducing ice-cold distilled water and neutralizing it with a 2M NaOH solution until reaching a pH of 7. The pH 7 point was marked by a pale-yellow precipitate that transitioned to white as the pH was further increased. Filtration separated the white precipitate, which was then washed multiple times with distilled water. NMR data: ^{1}H NMR (500 MHz, DMSO-d_6): δ ppm 9.2 (d, 1H), 8.5 (2d, 1H), 6.8 (s, 2H), 6.5 (d, 1H) **[Fig. S2]**.

Supporting information

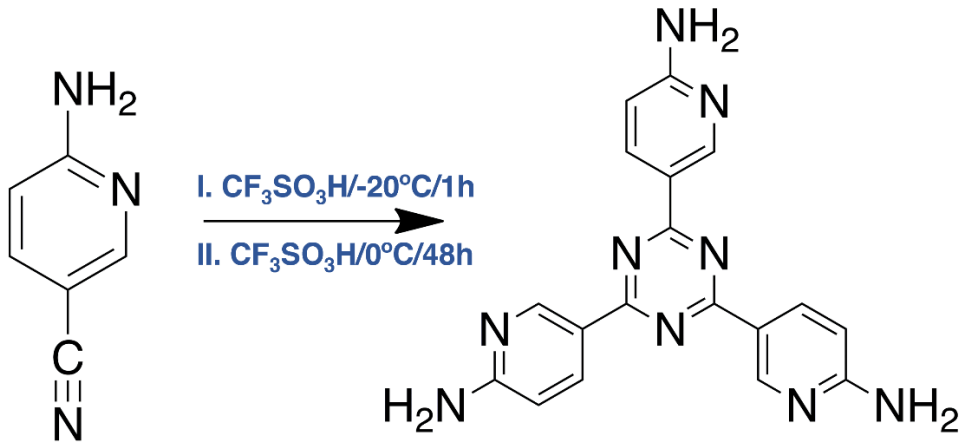

6-Amino-3-pyridinecarbonitrile **TAPT-N**

Scheme 2: Schematic diagram for synthesis of 5,5',5''-(1,3,5-triazine-2,4,6-triyl) tris(pyridin-2-amine) from 6-amino-3-pyridinecarbonitrile.

S2.3 Synthesis of TzCOF, CTzCOF and NTzCOF:

All the COFs were synthesized using solvothermal method via Schiff-base condensation.[2,3] In brief, for synthesizing TzCOF, a 10 mL Schlenk tube was charged with 21 mg of Tp (0.1 mmol) and 35.4 mg of TTA (0.1 mmol). Then, 1,4-dioxane (1 mL) and a certain amount of acetic acid were added to the tube. Then the mixture was sonicated for nearly 20 min followed by addition of 1 mL Mesitylene. The reaction mixture was then subjected to three freeze-pump-thaw (FPT) cycles and the sealed Schlenk tube was allowed to warm up to room temperature and then transferred to an oil bath kept at120 ºC. The reaction was left undisturbed for certain number of days at 120 ºC to yield TzCOF and CTzCOF.

Similarly, to synthesize NTzCOF, a similar synthetic procedure was followed using Tp (0.1 mmol, 21 mg) and amine (0.1 mmol, 35.7 mg).[2]

Note: The TzCOF possesses a semi-crystalline structure. We opted to refer to it as COF instead of a porous organic polymer (POP) to uphold uniformity and prevent any potential confusion among readers.

S3. Procedure for post-synthetic drug-loading and quantification of drug-loading capacity

Doxorubicin (DOX) was loaded to both the COFs namely TzCOF, CTzCOF and NTzCOF post-synthetically.[4] Briefly, 5 mg of COF dispersion was stirred in aqueous solution of DOX (10 mg/mL) for 24h at room temperature under dark.[5] Then the DOX-loaded COF was collected by centrifugation and washed with distilled water several times till the supernatant gets clear. Both the DOX-loaded COFs were named as DOX@TzCOFand DOX@NTzCOF. The quantification of loaded drug was done by using UV-Visible spectroscopy by recording

the absorbance of DOX before and after loading.[6,7] **(Fig. S8)** Finally, the drug-loading capacity was calculated using the formula given below.

$$\text{Drug-loading capacity (DLC)\%} = \frac{\text{wt. of loaded drug}}{\text{wt. of loaded drug + wt. of COF}} * 100$$

$$\text{Drug encapsulation efficiency (EE) \%} = \frac{\text{wt. of the loaded drug}}{\text{initial wt. of drug}} * 100$$

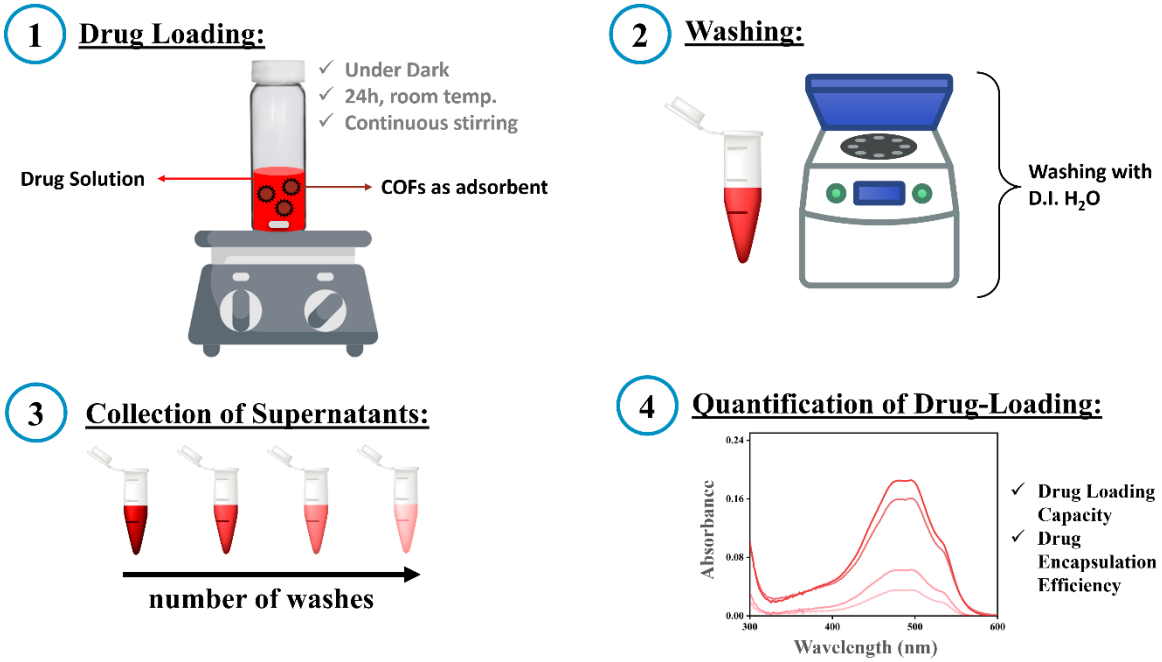

Scheme 3. Schematic representation of post-synthetic drug-loading to COFs.

S4. In-vitro biological studies for bare and drug-loaded COFs.

S4.1. Cell culture

All the cultures were maintained DMEM culture medium supplemented with 5% (v/v) FBS and 1% (v/v) antibiotic (100 U/mL Penicillin and 0.1 mg/mL Streptomycin along with 2 mM L-glutamine). The cultured cells were incubated and kept at 37 ºC in a humidified 5% CO_2 incubator. When the confluency reached 70-80%, the cells were seeded for further experiments.

S4.2. Biocompatibility analysis of TzCOF and NTzCOF

Biocompatibility of bare COFs was examined by MTT assay in HEK 293cells. The cells were seeded in 96-wells plate according to the requirement of the study. 10,000 cells were seeded in each well and allowed to adhere for 24 h in a humidified CO_2 incubator at 37 ºC. The cells were then treated with different concentrations of TzCOF and NTzCOF keeping the untreated control cells for comparison. Treated cells were again incubated in the humidified CO_2 incubator at 37 ºC for 24 h. After 24 h, MTT dye (10 µL) was added to each well and incubated for 3 h. The formazan crystals were solubilized by adding dimethyl sulfoxide (DMSO) to each well and absorbance was recorded at 570 nm wavelength using microplate reader.

Supporting information

S4.3. Cytotoxicity analysis of bare COFs, DOX@NTzCOF and DOX

A549 cells were seeded in a 96-wells plate at a density of 10,000 cells/well. The cells were allowed to adhere for 24 h in a humidified CO_2 incubator at 37 ºC. The cells were then treated with 10, 50 and 100 µg/mL of TzCOF, NTzCOF, DOX@NTzCOF and only DOX. The cells were further incubated for 24 h followed by MTT dye solution (10 µL, 5 mg/mL) addition and 3h of incubation. DMSO was added to solubilize formazan crystals and absorbance was recorded at 570 nm using microplate reader.

S4.4. Cellular uptake study of NTzCOF and DOX@NTzCOF

Confocal laser scanning microscopy (CLSM) was performed to study the time-dependent uptake of COF particles by A549 cancer cells. In brief, 50,000 cells were seeded on glass cover slip and allowed to adhere for 24 h in a humidified CO_2 incubator at 37 ºC. After this, cells were treated with 50 µg/mL each of NTzCOF, DOX@NTzCOF and DOX at corresponding concentration. The cells were incubated for different time duration of 3, 6, 9 and 12 h. Then the cells were fixed with 4% paraformaldehyde solution (200 µL, 20 min). The cells were gently washed three time with PBS and mounted on glass slide with mounting media.[8,9] The glass slide was then sealed, and the images were acquired by confocal microscope. The fluorescence intensity of internalized NTzCOF particles was measured using ImageJ software.

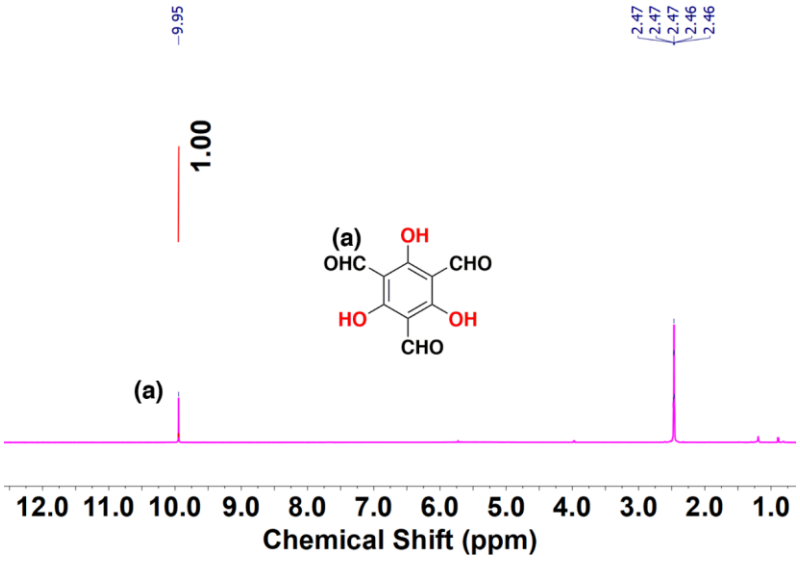

Fig. S1: ^{1}H NMR of triformyl phloroglucinol (Tp).

Supporting information

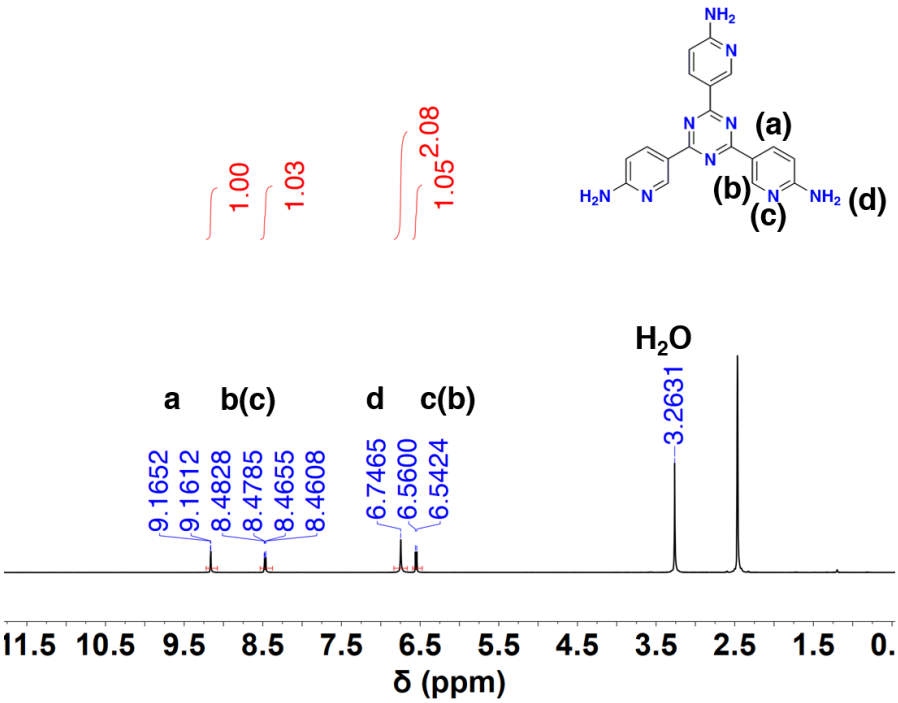

Fig. S2: ^{1}H NMR of 5,5',5''-(1,3,5-triazine-2,4,6-triyl)tris(pyridin-2-amine).

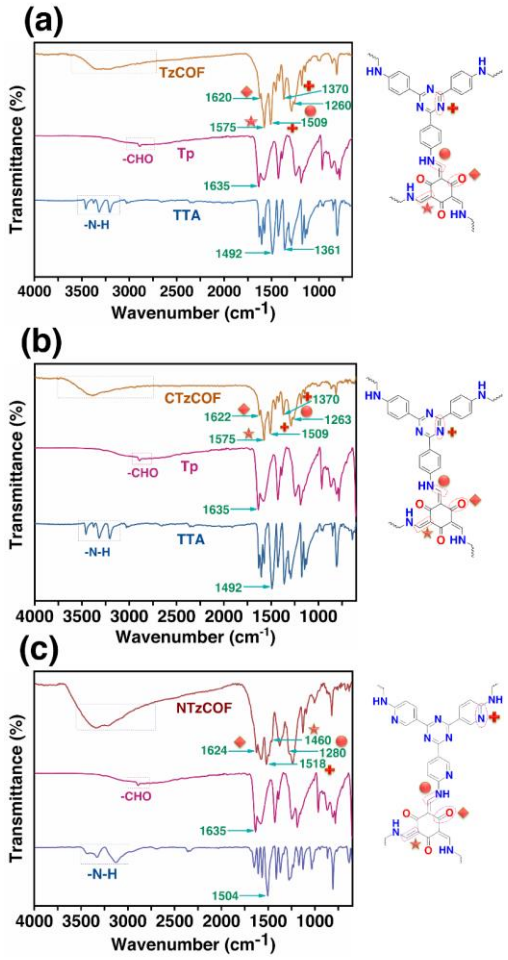

Supporting information

Fig. S3: (a) FTIR spectra for TzCOF, (b) CTzCOF and (c) NTzCOF. The symbols given with each peak position indicate towards the corresponding functional group stretch in COF-unit. The peak near to1620-1624 cm^{-1} corresponds to -C=O stretch in all COFs, while the peak near to 1575 cm^{-1} and 1255 cm^{-1} indicate -C=C- and -C-N- bond stretching respectively in (a) TzCOF and (b) CTzCOF. While peaks nearly at 1460 cm^{-1} and 1280 cm^{-1} correspond to C=C and C-N bond stretching respectively in (c) NTzCOF. The peaks nearly at 1370 cm^{-1} and 1509-1518 cm^{-1} correspond to triazine ring.[10,2] Absence of characteristic peaks for C=N bond suggests tautomerization to enamine form. The dotted box indicates that no monomers are present in synthesized COFs.

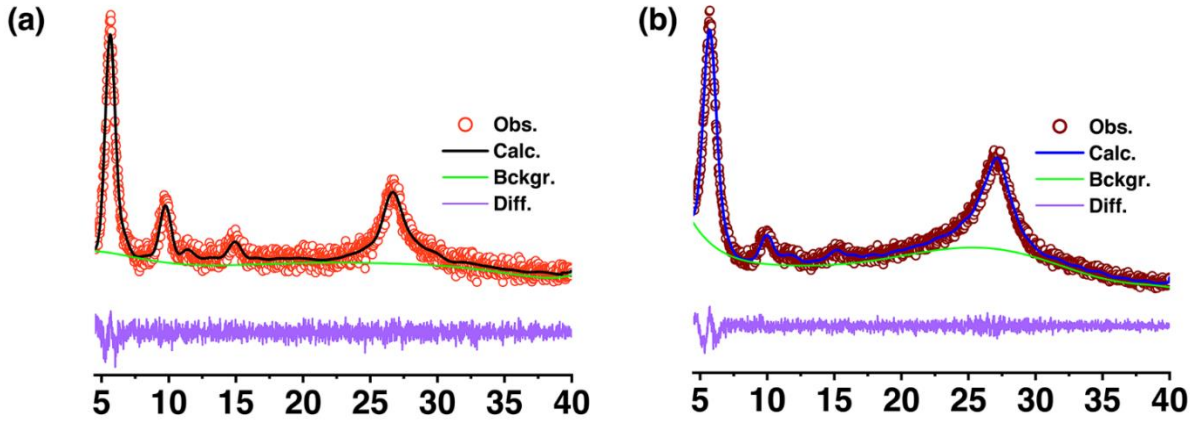

Fig. S4: Rietveld refinement of the Powder X-ray diffraction pattern of (a) CTzCOF and (b) NTzCOF. Orange and brown line represents the experimental data. The black and blue line represents the calculated fit. The purple line is the difference curve and the green line shows the background.[11]

Table S1: Structural parameters from the experimental PXRD patterns and the Rietveld Refinement profiles.

COF	**2Θ (°)**	**Corresponding reflection plane**	**FWHM**	**Rietveld Refined Cell Parameters**				
				a	**b**	**c**	**ILD**	χ^2
TzCOF	5.7	100	1.09	-	-	-	-	-
CTzCOF	5.7	100	0.9	18.1140(1)	18.1797(1)	13.4883(1)	3.37	1.603
NTzCOF	5.7	100	0.98	18.1790(1)	18.4587(1)	13.4211(1)	3.36	1.397

Supporting information

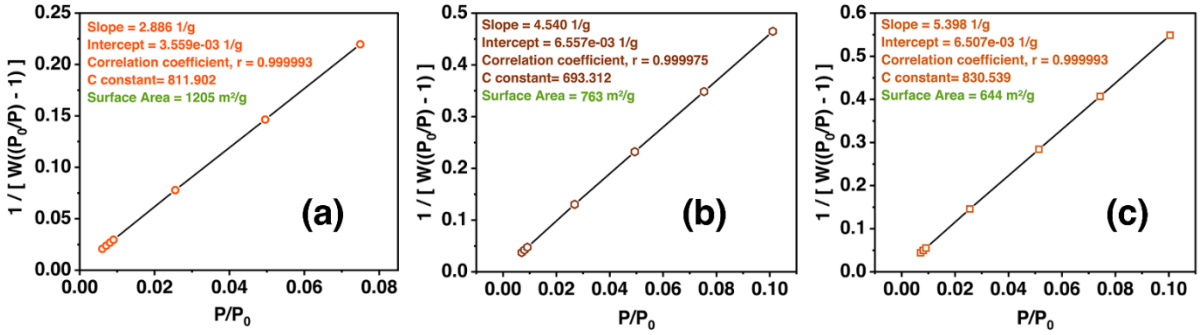

Fig. S5: Multipoint BET plot of (a) CTzCOF, (b) NTzCOF and (c) TzCOF.

Table S2: Surface areas of COFs calculated from the N_2 sorption isotherm at 77 K.

Sample	BET Surface Area (m^2/g)	Langmuir Surface Area (m^2/g)	Microporous Surface Area (de-boer method) (m^2/g)	External Surface Area (de-boer method) (m^2/g)	Micropore Volume (V_m) (cc/g)	QSDFT Pore Size (nm)
TzCOF	644	888	334	310	0.14	1.453
NTzCOF	763	1058	415	348	0.18	1.403
CTzCOF	1205	1543	891	314	0.37	1.503

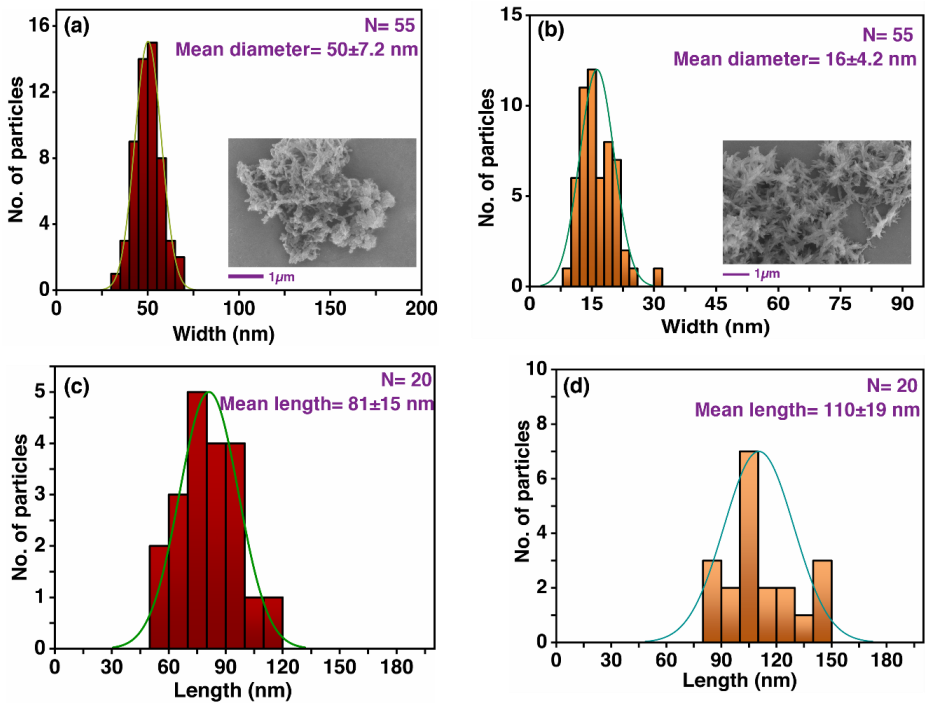

Fig. S6 Histogram showing mean diameter and length of (a,c) NTzCOF nanofibres and (b,d) TzCOF nanofibres analysed using SEM images and ImageJ software.

Supporting information

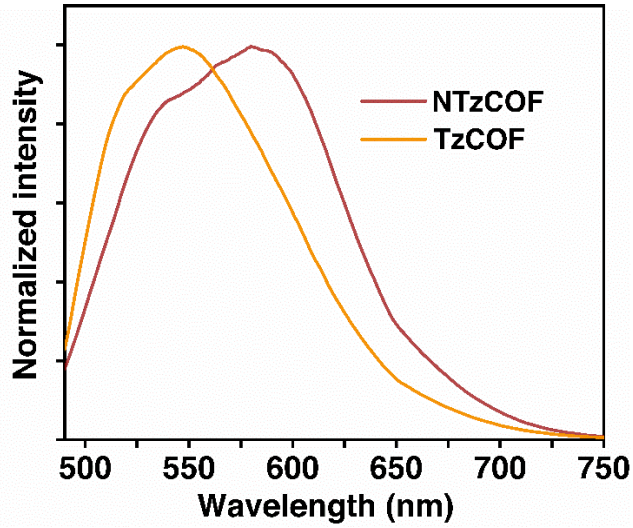

Fig. S7 Liquid-state fluorescence spectrum of TzCOF and NTzCOF in water. (Excitation wavelength, λ_{ex} = 472 nm for NTzCOF and 425 nm for TzCOF)

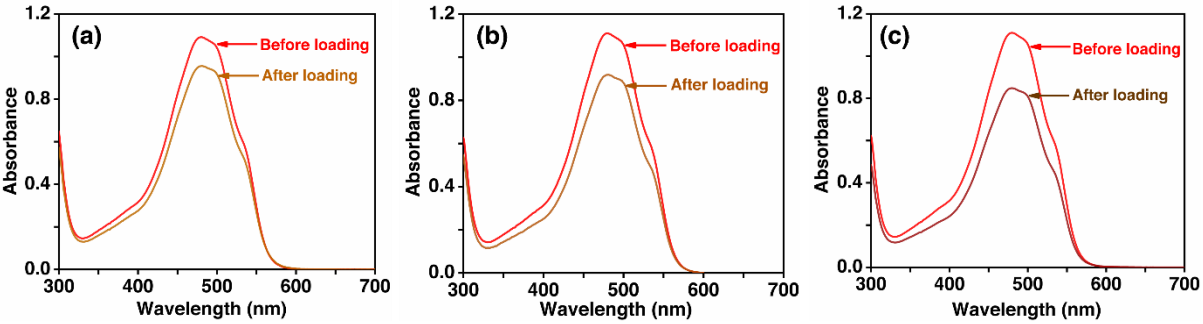

Fig. S8 UV-Visible absorbance spectra of DOX before and after loading to (a) TzCOF, (b) CTzCOF and (c) NTzCOF along with three washing profiles.

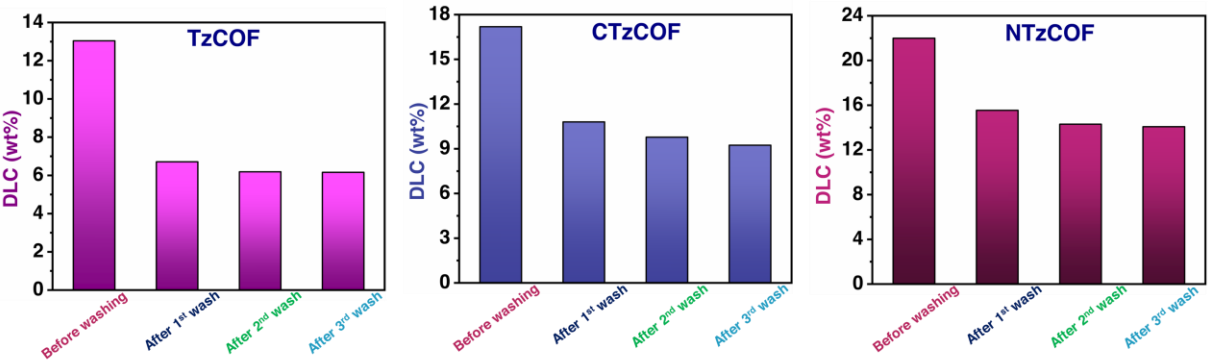

Fig. S9: Bar plots showing drug loading capacity (DLC) after post-synthetic DOX loading with subsequent washing profiles.

Supporting information

Table S3: Comparison of DLC and DEE of three COFs with other porous materials for DOX delivery along with the cytotoxicity of bare and drug-loaded material.

Material		**DLC (wt%)**	**DEE (%)**	**Cytotoxicity of bare material (24 h)**	**Cytotoxicity of drug-loaded material (24 h)**	**Ref.**
Category	**Name**					
Mesoporous silica nanoparticles (MSNs)	MSNs–SS–PEG	12.3	88.2	Negligible up to 100 μg mL^{-1}	<30% at 10 μg mL^{-1}	[12]
	Fe_3O_4@$mSiO_2$	20	100	Negligible up to 100 μg mL^{-1}	~55% at 20 μg mL^{-1} equ. DOX concentration	[13]
	MSNs-CS/CMC	22	79	Negligible up to 100 μg mL^{-1}	40% at 50 μg mL^{-1}	[14]
Mesoporous carbon nanoparticles (MCNs)	HMC-SS-PAA	51.9	NA	Negligible up to 10 μg mL^{-1}	~70% death at 10 μg mL^{-1}	[15]
Metal organic frameworks (MOFs)	UCNPs@MOF	17.2	NA	Negligible at 100 μg mL^{-1}	~20% at 50 μg mL^{-1}	[16]
	Gd-pDBI	12	NA	~10% at 100 μg mL^{-1}	~50% at 100 ug mL^{-1}	[17]
Zeolitic imidazolate framework	Fe_3O_4-ZIF-8	12	NA	<10% up to 80 μg mL^{-1}	>80% at 80 μg mL^{-1} (9.6 μg mL^{-1} DOX)	[18]
	PAA@ZIF-8	65.5	95	~10% up to 50 μg mL^{-1}	~80% at 50 μg mL^{-1}	[19]
Porous silicon nanoparticles	BSA/D-PSiNP nanocomposites	19.35	NA	~10% up to 20 μg mL^{-1}	~90% at 20 μg mL^{-1}	[20]
Porous covalent triazine polymer	NCTP	20	NA	<10% at 100 μg mL^{-1}	~90% at 20 μg mL^{-1}	[21]
	HY/SS-CONs	18	NA	<10% at 100 μg mL^{-1}	~70% at 40 μg mL^{-1}	[22]
	NTzCOF	Before washing= 21.99 After washing= 14.08	98.58	<10% up to 100 μg mL^{-1}	~70% at 50 μg mL^{-1} (7 μg mL^{-1} of DOX)	This work

Supporting information

Covalent organic frameworks	CTzCOF	Before washing= 17.19	99.41	NA	NA	This work
		After washing= 9.12				
	TzCOF	Before washing= 13.04	97.12	Negligible at 100 μg mL^{-1}	NA	This work
		After washing= 6.16				

Evidently, the comparison of DLC and its impact on cytotoxicity of the drug loaded vehicle is not straight forward. There are many different materials such as mesoporous silica, other COFs, metal organic frameworks, mesoporous carbon and porous polymers reported for the encapsulation of DOX. Many such porous materials, for example mesoporous carbon (HMC-SS-PAA) and MOF (PAA@ZIF-8) are reported to have very high drug loading of DOX, because of the strong interaction between the carrier and the drug. However, the cytotoxicity of these drug-loaded nanocarriers is similar to NTzCOF presented in this study (~70 % at 50 μg mL^{-1}). Hence, it can be concluded that the nanocarrier NTzCOF presented in this study performed well in in-vitro biological studies.

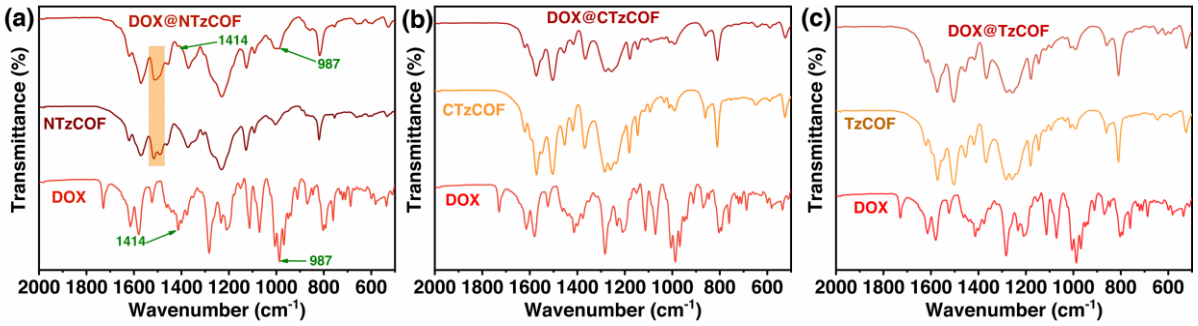

Fig. S10: FTIR spectra of (a) DOX-loaded NTzCOF (b) DOX-loaded CTzCOF and (c) DOX-loaded TzCOF along with DOX and pristine COF. Emergence of FTIR peaks at 1414 and 987 cm^{-1} in the DOX loaded NTzCOF confirms the presence of the drug molecule inside the pores.[23] Change of peak at 1518 cm^{-1} (aromatic -C=N-)[2] of DOX@NTzCOF as compared to NTzCOF indicates that DOX is interacting with pyridyl N-atom. However, there was only negligible change in the peak at 1503 cm^{-1} (-C=N functionality, triazine)[10] of DOX@CTzCOF and DOX@TzCOF as compared to pristine COFs. This indicates a minimum level of interaction between DOX and the triazine ring of the COFs.

Supporting information

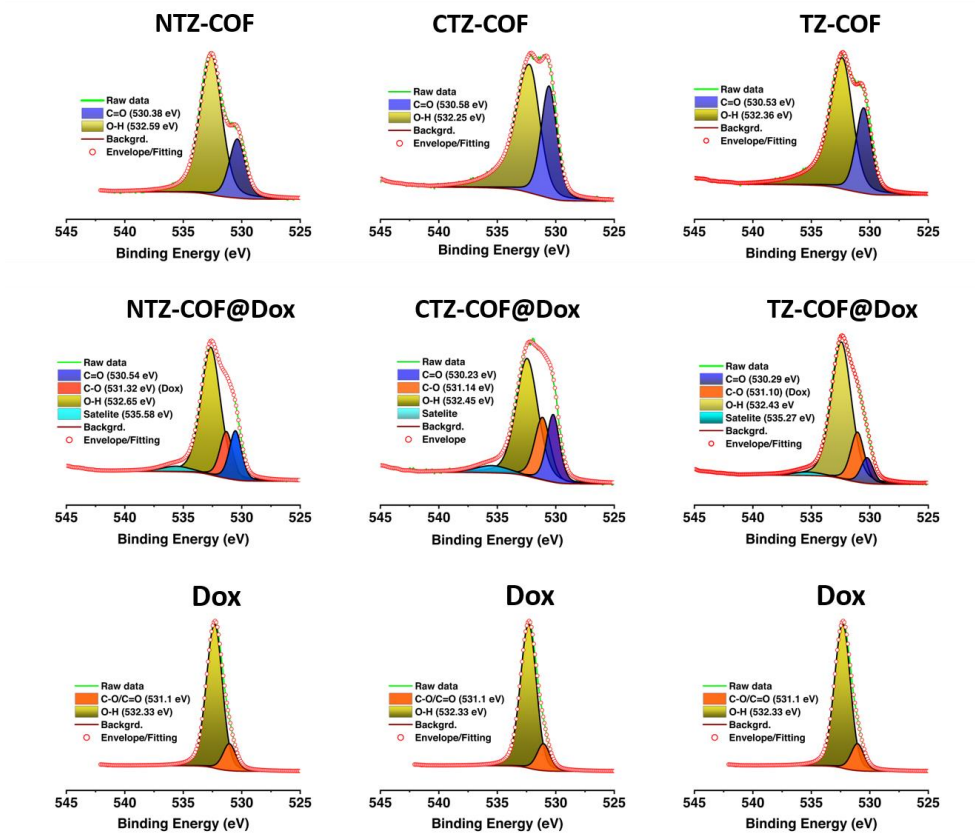

Fig. S11: O1s XPS spectra of three pristine COFs, DOX-loaded COFs and DOX. Spectra of pristine COFs shows the signals around ~530 eV and ~532 eV indicating the presence of C=O and O-H functionalities respectively.[24,25] The XPS signal originating from the C-O bonds of the DOX molecule exhibited a more pronounced shift in the case of Dox@NTzCOF as compared to Dox@CTzCOF and Dox@TzCOF. In particular, the binding energy value shifted 0.22 eV for the case of Dox@NTzCOF, whereas the shift was insignificant for the other two nanocarriers after Dox loading.

Supporting information

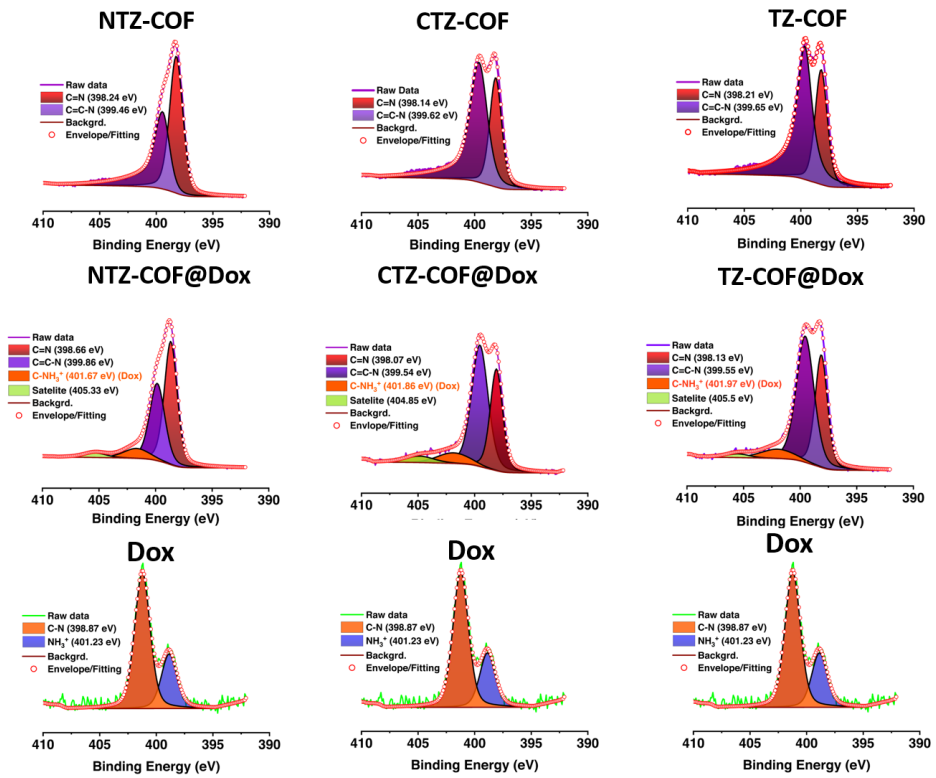

Fig. S12: N1s XPS spectra of three pristine COFs, DOX-loaded COFs and DOX. The signals around 398 eV and 399 eV in pristine COFs (Fig. R3) can be ascribed to C=N (pyridinic/triazine) and C=C-N (enamine) bonds.[26,25,27]

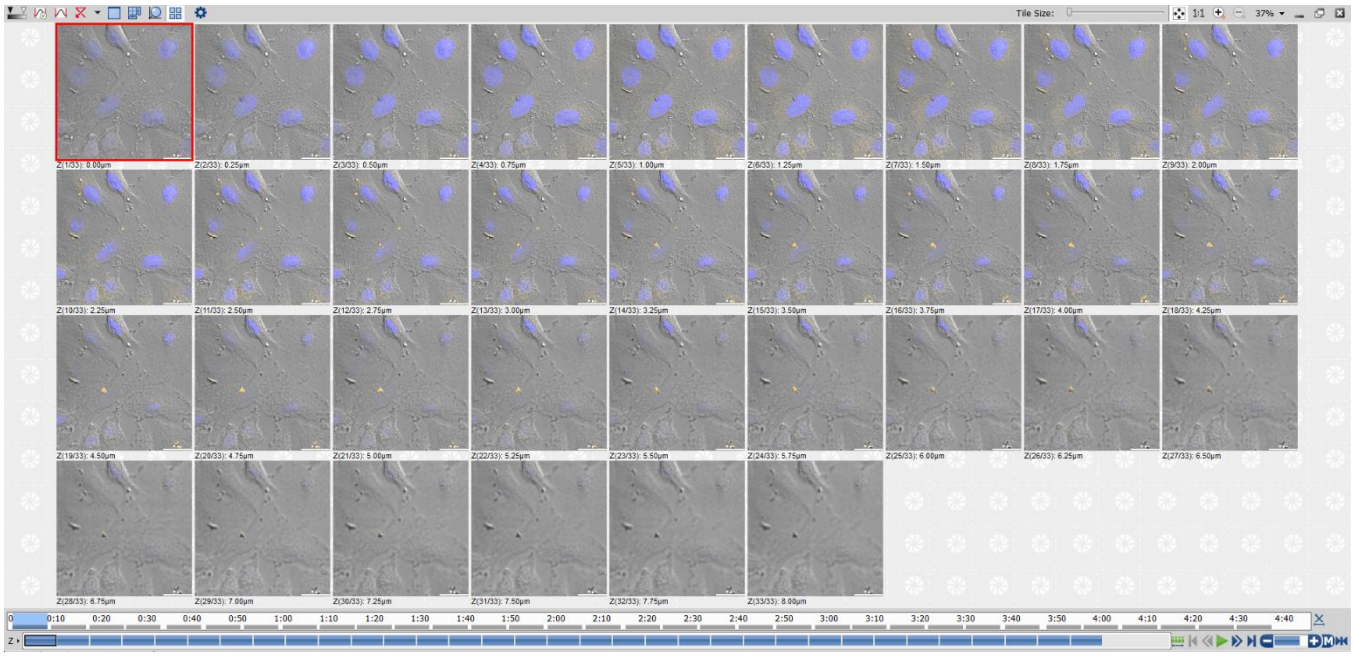

Fig.S13 Confocal images of A549 cells treated with NTzCOF at different z-height.

Supporting information

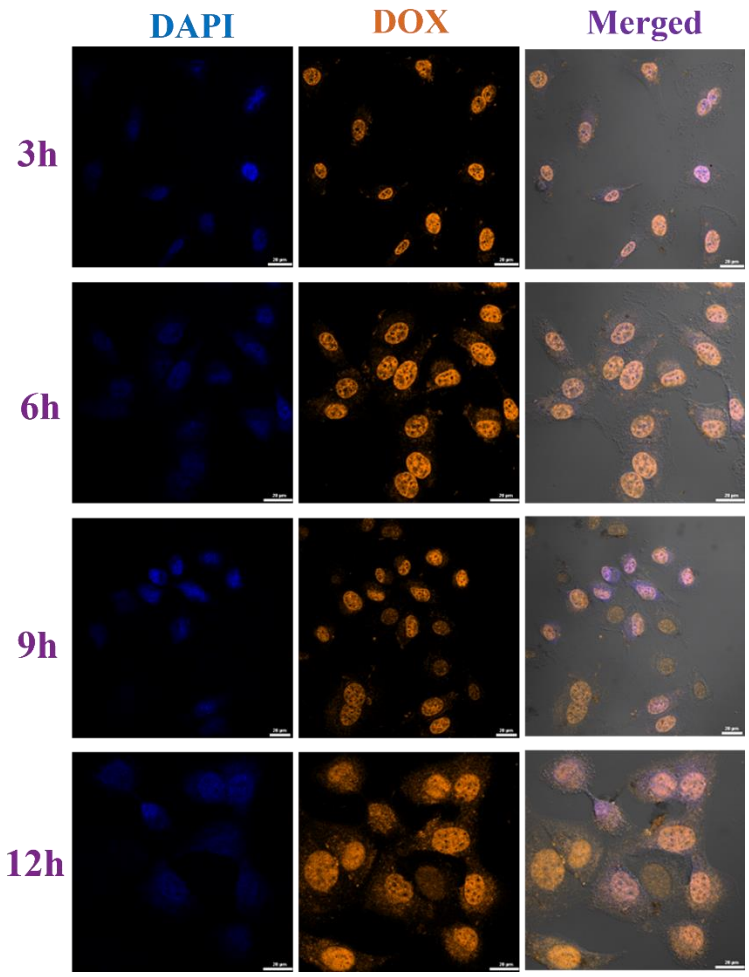

Fig.S14 Confocal images of A549 cells treated with DOX at different time intervals.

References:

1 C. V Yelamaggad, A. S. Achalkumar, D. S. S. Rao and S. K. Prasad, Luminescent, Liquid Crystalline Tris(N-salicylideneaniline)s: Synthesis and Characterization, *J. Org. Chem.*, 2009, **74**, 3168–3171.

2 S. Haldar, R. Kushwaha, R. Maity and R. Vaidhyanathan, Pyridine-Rich Covalent Organic Frameworks as High-Performance Solid-State Supercapacitors, *ACS Mater. Lett.*, 2019, **1**, 490–497.

3 W. Li, C.-X. Yang and X.-P. Yan, A versatile covalent organic framework-based platform for sensing biomolecules, *Chem. Commun.*, 2017, **53**, 11469–11471.

4 Y. Liu, G. Yang, S. Jin, L. Xu and C.-X. Zhao, Development of High-Drug-Loading Nanoparticles, *Chempluschem*, 2020, **85**, 2143–2157.

5 P. Gao, X. Shen, X. Liu, Y. Chen, W. Pan, N. Li and B. Tang, Nucleic Acid-Gated Covalent Organic Frameworks for Cancer-Specific Imaging and Drug Release, *Anal. Chem.*, 2021, **93**, 11751–11757.

6 K. Radhakrishnan, M. B. Thomas, S. Pulakkat, D. P. Gnanadhas, D. Chakravortty and

Supporting information

A. M. Raichur, Stimuli-responsive protamine-based biodegradable nanocapsules for enhanced bioavailability and intracellular delivery of anticancer agents, *J. Nanoparticle Res.*, 2015, **17**, 341.

7 M. Li, Y. Peng, F. Yan, C. Li, Y. He, Y. Lou, D. Ma, Y. Li, Z. Shi and S. Feng, A cage-based covalent organic framework for drug delivery, *New J. Chem.*, 2021, **45**, 3343–3348.

8 M. Alvarado-kristensson, MethodsX A simple and fast method for fi xation of cultured cell lines that preserves cellular structures containing gamma-tubulin, *MethodsX*, 2018, **5**, 227–233.

9 C. Fixation, h i t e a p e r Sample Preparation for Fluorescence Microscopy : An Introduction Concepts and Tips for Better Fixed Sample Imaging Results.

10 R. Gomes and A. Bhaumik, A new triazine functionalized luminescent covalent organic framework for nitroaromatic sensing and CO2 storage, *RSC Adv.*, 2016, **6**, 28047–28054.

11 B. H. Toby, EXPGUI, a graphical user interface for GSAS, *J. Appl. Crystallogr.*, 2001, **34**, 210–213.

12 H. Gong, Z. Xie, M. Liu, H. Zhu and H. Sun, Redox-sensitive mesoporous silica nanoparticles functionalized with PEG through a disulfide bond linker for potential anticancer drug delivery, *RSC Adv.*, 2015, **5**, 59576–59582.

13 Y. Chen, H. Chen, D. Zeng, Y. Tian, F. Chen, J. Feng and J. Shi, Core/Shell Structured Hollow Mesoporous Nanocapsules: A Potential Platform for Simultaneous Cell Imaging and Anticancer Drug Delivery, *ACS Nano*, 2010, **4**, 6001–6013.

14 L. Cui, W. Liu, H. Liu, Q. Qin, S. Wu, S. He, X. Pang, C. Zhu and P. Shen, pH-Triggered Charge-Reversal Mesoporous Silica Nanoparticles Stabilized by Chitosan Oligosaccharide/Carboxymethyl Chitosan Hybrids for Effective Intracellular Delivery of Doxorubicin, *ACS Appl. Bio Mater.*, 2019, **2**, 1907–1919.

15 X. Li, C. Liu, S. Wang, J. Jiao, D. Di, T. Jiang, Q. Zhao and S. Wang, Poly(acrylic acid) conjugated hollow mesoporous carbon as a dual-stimuli triggered drug delivery system for chemo-photothermal synergistic therapy, *Mater. Sci. Eng. C*, 2017, **71**, 594–603.

16 K. Deng, Z. Hou, X. Li, C. Li, Y. Zhang, X. Deng, Z. Cheng and J. Lin, Aptamer-Mediated Up-conversion Core/MOF Shell Nanocomposites for Targeted Drug Delivery and Cell Imaging, *Sci. Rep.*, 2015, **5**, 7851.

17 T. Kundu, S. Mitra, P. Patra, A. Goswami, D. Díaz Díaz and R. Banerjee, Mechanical downsizing of a gadolinium (III)-based metal–organic framework for anticancer drug delivery, *Chem. Eur. J.*, 2014, **20**, 10514–10518.

18 C. Cheng, C. Li, X. Zhu, W. Han, J. Li and Y. Lv, Doxorubicin-loaded Fe3O4-ZIF-8 nano-composites for hepatocellular carcinoma therapy, *J. Biomater. Appl.*, 2019, **33**, 1373–1381.

Supporting information

19 H. Ren, L. Zhang, J. An, T. Wang, L. Li, X. Si, L. He, X. Wu, C. Wang and Z. Su, Polyacrylic acid@zeolitic imidazolate framework-8 nanoparticles with ultrahigh drug loading capability for pH-sensitive drug release, *Chem. Commun.*, 2014, **50**, 1000–1002.

20 B. Xia, W. Zhang, J. Shi and S. Xiao, A novel strategy to fabricate doxorubicin/bovine serum albumin/porous silicon nanocomposites with pH-triggered drug delivery for cancer therapy in vitro, *J. Mater. Chem. B*, 2014, **2**, 5280–5286.

21 A. Rengaraj, P. Puthiaraj, Y. Haldorai, N. S. Heo, S.-K. Hwang, Y.-K. Han, S. Kwon, W.-S. Ahn and Y. S. Huh, Porous covalent triazine polymer as a potential nanocargo for cancer therapy and imaging, *ACS Appl. Mater. Interfaces*, 2016, **8**, 8947–8955.

22 C. Wang, H. Liu, S. Liu, Z. Wang and J. Zhang, pH and Redox dual-sensitive covalent organic framework nanocarriers to resolve the dilemma between extracellular drug loading and intracellular drug release, *Front. Chem.*, 2020, **8**, 488.

23 R. Bansal, R. Singh and K. Kaur, Quantitative analysis of doxorubicin hydrochloride and arterolane maleate by mid IR spectroscopy using transmission and reflectance modes, *BMC Chem.*, 2021, **15**, 27.

24 H. Wang, E. Almatrafi, Z. Wang, Y. Yang, T. Xiong, H. Yu, H. Qin, H. Yang, Y. He, C. Zhou, G. Zeng and P. Xu, Self-assembly hybridization of COFs and g-C3N4: Decipher the charge transfer channel for enhanced photocatalytic activity, *J. Colloid Interface Sci.*, 2022, **608**, 1051–1063.

25 X. Han, F. Zhao, Q. Shang, J. Zhao, X. Zhong and J. Zhang, Effect of Nitrogen Atom Introduction on the Photocatalytic Hydrogen Evolution Activity of Covalent Triazine Frameworks: Experimental and Theoretical Study, *ChemSusChem*, 2022, **15**, e202200828.

26 D. Y. Osadchii, A. I. Olivos-Suarez, A. V Bavykina and J. Gascon, Revisiting Nitrogen Species in Covalent Triazine Frameworks, *Langmuir*, 2017, **33**, 14278–14285.

27 C. R. DeBlase, K. E. Silberstein, T.-T. Truong, H. D. Abruña and W. R. Dichtel, β-Ketoenamine-Linked Covalent Organic Frameworks Capable of Pseudocapacitive Energy Storage, *J. Am. Chem. Soc.*, 2013, **135**, 16821–16824.